Journal of Power Sources 230 (2013) 236–243

Contents lists available at SciVerse ScienceDirect

Journal of Power Sources

journal homepage: www.elsevier.com/locate/jpowsour

Carbon corrosion and platinum nanoparticles ripening under open circuit potential conditions

Z. Zhao [a,1], L. Castanheira [a,1], L. Dubau [a,1], G. Berthomé [b], A. Crisci [c], F. Maillard [a,*,1]

[a] Laboratoire d'Electrochimie et de Physico-chimie des Matériaux et des Interfaces, UMR 5279 CNRS, Grenoble INP, Université de Savoie, Université Joseph Fourier, 1130 rue de la piscine, BP 75, 38402 Saint Martin d'Hères Cedex, France
[b] Science et Ingénierie des MAtériaux et Procédés, UMR 5266 CNRS, Grenoble INP, Université Joseph Fourier, BP 75, 38402 Saint Martin d'Hères Cedex, France
[c] Consortium des Moyens Technologiques Communs de Grenoble INP, 1260, rue de la piscine, BP 75, 38402 Saint Martin d'Hères Cedex, France

HIGHLIGHTS

- Degradation mechanism of Pt/Vulcan XC 72 nanoparticles at open circuit potential.
- The amorphous domains of Vulcan XC 72 are easily oxidized into CO_2.
- CO_2 formation is kept to a low extent on the organized domains of Vulcan XC 72.
- The Pt-catalysed carbon corrosion yields aggregation/detachment of the Pt particles.

ARTICLE INFO

Article history:
Received 4 September 2012
Received in revised form
8 December 2012
Accepted 14 December 2012
Available online 22 December 2012

Keywords:
Proton-exchange membrane fuel cell
Durability
Degradation mechanism
Carbon corrosion, high surface area carbon support
Oxygen-containing carbon surface groups
Pt nanoparticles

ABSTRACT

This study bridges the structural and the chemical properties of a high surface area carbon support (Vulcan XC72) used in proton-exchange membrane fuel cells and its resistance to corrosion under open circuit potential (OCP). Inks composed of Pt/XC72 electrocatalysts, Nafion® ionomer and water were aged for 3.5 years under air atmosphere. These conditions cause a mixed potential produced by simultaneous carbon support corrosion and oxygen reduction on Pt. Raman, X-ray photoelectron and Fourier Transform infrared spectroscopy measurements show that the amorphous domains of the Vulcan XC72 support are preferentially oxidized into CO_2 during the first 1.5 years of aging at OCP. A much sluggish corrosion rate of the organized domains of the Vulcan XC72 support is observed by Raman and X-ray photoelectron spectroscopy measurements. Fourier-Transformed infrared spectroscopy results indicate that the corrosion of the organized domains of the carbon support produces mostly oxygen-bearing carbon surface groups, and to a minor extent, CO_2 molecules at $U = 0.80$ V *vs.* RHE. Electron microscopy and electrochemical techniques were used to monitor the morphological changes of the Pt nanoparticles over time, resulting from the Pt-catalysed carbon corrosion.

1. Introduction

Proton-exchange membrane fuel cells (PEMFCs) attract much attention as a viable solution to curb our energy-related CO_2 emissions [1]. They directly convert the chemical energy of a fuel into electrical energy from the reaction with oxygen, without the intermediate formation of heat and mechanical energy as in conventional Carnot cycle-based engines. PEMFCs use porous electrodes made of ionomer-bonded carbon-supported Pt-based nanoparticles to accelerate the kinetics of the electrochemical hydrogen oxidation reaction (HOR) at the anode, and of the sluggish oxygen reduction reaction (ORR) at the cathode. However, four catalyst degradation mechanisms modify their structure, and yield electrochemically active surface area (ECSA) loss during PEMFC operation: (i) metal nanoparticle aggregation and/or detachment [2–6], (ii) corrosion of the high surface area carbon (HSAC) support [7–10], (iii) 3D Ostwald ripening, where the smallest Pt crystallites dissolve preferentially, yielding the formation of Pt^{z+} ions and their redeposition onto larger particles [2,11–13]; and (iv) chemical reduction of the Pt^{z+} ions in ion conductors, leading electrically disconnected Pt crystallites [2,11–13].

Which mechanism is contributing most to the loss of ECSA strongly depends on the initial size of the Pt-based crystallites, the robustness of the carbon support and the PEMFC operating conditions. At the anode (reducing electrode potential and gas

* Corresponding author. Tel.: +33 0 476 82 65 88; fax: +33 0 476 82 67 77.
E-mail address: frederic.maillard@lepmi.grenoble-inp.fr (F. Maillard).
[1] ISE active member.

0378-7753/$ – see front matter © 2012 Elsevier B.V. All rights reserved.
http://dx.doi.org/10.1016/j.jpowsour.2012.12.053

atmosphere), Ostwald ripening and carbon corrosion play a minor role, but recent evidences were brought that Pt nanocrystallites migrate/aggregate over [3] or even detach from [5,14] the carbon support. At the cathode (oxidizing electrode potential and gas atmosphere, presence of water), both the carbon support and the Pt-based nanoparticles are covered by surface oxides and thus unstable. Ostwald ripening and carbon corrosion are believed to be the major degradation mechanisms at this electrode [13–16]. The HSAC corrosion kinetics is rather sluggish at conventional PEMFC cathode operation potential, but is significantly increased at $U > 1$ V *vs.* RHE [9,10,17] or during electrode potential transients [5,18]. Unfortunately, the HSAC support and the metal nanoparticles negatively interact with each other to accelerate the ECSA losses. A recent study by electrochemical – Fourier transform infrared spectroscopy showed that carbon surface oxide species present on HSAC are dehydrogenated at low electrode potential $U < 0.60$ V vs. RHE on Pt/C, yielding the formation of CO/Pt [9]. At higher electrode potential $U > 0.60$ V vs. RHE, the formation of surface oxides on Pt facilitates the removal of the CO molecules and accelerates the carbon corrosion kinetics [9,10,19]. Clearly, the corrosion of the carbon support will also facilitate the detachment/aggregation of the Pt nanoparticles.

A large part of our knowledge on the durability of PEMFC materials arises from accelerated durability tests (ADTs). Such tests combine variations of the electrode potential, the temperature, the relative humidity and the gas composition, yielding fast variations of the ECSA. Although very informative, they cause the occurrence of simultaneous degradation mechanisms (dissolution, redeposition, HSAC support corrosion, particle detachment, aggregation), and remain poorly informative from a mechanistic viewpoint. In particular, little is known about the effect of high cathode potential experienced by the cathodic electrocatalyst in PEMFC stacks during idle conditions (*i.e.* the time when only idle auxiliary load power is drawn from the stack) or open circuit voltage (during fuel cell shut-down). These conditions yield cathode potential close to 0.90 or 1.00 V *vs.* RHE, respectively and induce carbon weight losses over time [17,20].

In this study, suspensions composed of Pt/Vulcan XC72 powder, solid ionomer and water were aged for 3.5 years under air atmosphere. These conditions cause a mixed potential produced by simultaneous carbon support corrosion and oxygen reduction on Pt, and hence are believed to reproduce to some extent what happens in a PEMFC cathode at OCP or under idling conditions. X-ray Photoelectron Spectroscopy (XPS), Raman spectroscopy and EC-FTIR measurements were used to monitor the structural and chemical changes associated with the carbon oxidation reaction (COR), and gain some insights into the reaction mechanism. Physical (high-resolution transmission electron microscopy) and electrochemical (cyclic voltammetry) techniques were used to monitor the changes in morphology and size of the supported Pt nanoparticles.

2. Experimental

2.1. Catalysts

Three samples based on Pt nanoparticles supported on Vulcan XC72 with different weight fractions (wt. %) of 20, 30 and 40%, translating into surface averaged particle size of 2.9, 3.4 and 4.7 nm, respectively (see Table 1) were supplied by E-Tek. The catalysts were used as-received without any further treatment.

2.2. High-resolution transmission electron microscopy imaging

The metal nanoparticles were examined with a Jeol 2010 TEM operated at 200 kV with a point to point resolution of 0.19 nm. The TEM images were used to build the particle size distribution of the catalysts before/after electrochemical treatment. From these observations, the number averaged diameter:

$$\overline{d}_N = \frac{\sum_{i=1}^{n} n_i d_i}{\sum_{i=1}^{n} n_i} \quad (1)$$

and the surface averaged diameter:

$$\overline{d}_S = \frac{\sum_{i=1}^{n} n_i d_i^3}{\sum_{i=1}^{n} n_i d_i^2} \quad (2)$$

were determined by eye-counting over *ca.* 400 particles (n_i stands for the number of particles having a diameter d_i). Only "isolated" particles (that is non-aggregated, single grain spherical particles) were counted to build the PSD. We also used TEM images to evaluate the number of isolated/aggregated particles per μm^2 of carbon, by eye-counting over typically 20 representative images (*ca.* 500 particles).

2.3. Electrochemical measurements in liquid electrolyte

2.3.1. Solutions

All the glassware used in this study was cleaned by immersion in a H_2SO_4:H_2O_2 mixture overnight and thoroughly rinsed with MQ-grade water. Solutions were prepared from ultrapure water (MQ grade, 18.2 MΩ cm, 1–3 ppm TOC) and $HClO_4$ (Suprapur, Merck). The electrolyte was a 0.1 M $HClO_4$ solution purged with argon (99.99%).

2.3.2. Preparation and aging of catalysts inks

Catalyst inks composed of 5.0 mg of Pt/C, 2.4 mL of MQ-grade water and 54 μL of 5 wt. % Nafion® solution (Electrochem. Inc.) were prepared in glass flasks and ultrasonically treated for 30 min to obtain homogeneous dispersions. The glass flasks were sealed

Table 1
Evolution of the number and surface averaged mean particle size, the density of isolated and aggregated particles and the loss of isolated Pt particles for three Pt/C commercial electrocatalysts during a 3.5 years period at open circuit potential conditions.

	20 wt. % Pt/C		30 wt. % Pt/C		40 wt. % Pt/C			
	Fresh	After 2.5 years at OCP	Fresh	After 2.5 years at OCP	Fresh	After 1.5 years at OCP	After 2.5 years at OCP	After 3.5 years at OCP
$\overline{d}_N$/nm	2.5	2.6	2.7	2.8	3.5	3.8	3.6	3.6
$\overline{d}_S$/nm	2.9	3.1	3.4	3.6	4.5	4.9	4.8	5.1
Number of isolated particles/μm^{-2} carbon	38,000	33,000	10,800	8600	8000	6700	4300	2200
Number of aggregated particles/μm^{-2} carbon	2500	2600	2800	2500	2600	2100	2200	2500
Total number of particles/μm^{-2} carbon	40,500	35,600	13,600	11,100	10,600	8800	6500	4700
Fraction of aggregated particles/%	6.2	7.3	20.6	22.5	24.5	23.9	33.8	53.2
Loss of isolated particles/%	0	13.2	0	20.4	0	16.3	46.3	72.5

and stored for different durations. However, they remain permeable to air, which causes a mixed electrode potential composed of anodic current (carbon support corrosion) and cathodic current (oxygen reduction on Pt). The aged catalysts inks were used for electrochemical, chemical and physical characterizations after constant intervals of time ranging from 1.5 years to 3.5 years.

2.3.3. Electrochemical cell set-up

An aliquot of the fresh/aged ink was deposited onto a glassy carbon (Sigradur, 0.196 cm^2) or a gold disk (in EC-FTIR experiments) and sintered for 5 min at $T = 383$ K to ensure its binding to the disk and evaporation of the Nafion® solvents. The resulting thin film electrode was immersed in the electrochemical cell at controlled electrode potential ($U = 0.10$ V *vs.* the reversible hydrogen electrode (RHE)), and used as a working electrode. The counter-electrode was a Pt foil and the reference electrode - a mercury sulphate electrode (MSE) $Hg|Hg_2SO_4$, K_2SO_4 (saturated) connected to the cell via a Luggin capillary. More details are available in Ref. [21].

2.4. Fourier-transformed infrared spectroscopy coupled in situ with electrochemical measurements

Coupled EC-FTIR experiments were performed in external reflection mode with a home-made electrochemical cell and *p*-polarized light at $T = 20 \pm 2$ °C. A CaF_2 prism, beveled at 60°, constituted the bottom of the cell. The spectrometer was a Bruker Vertex 80v spectrometer and the detector a liquid N_2-cooled mercury–cadmium–telluride. The spectrometer was kept under vacuum during the experiments. The spectral resolution was set to 4 cm^{-1} and 256 interferograms were co-added and then Fourier-transformed to obtain a single-beam spectrum (acquisition of one single-beam spectrum takes *ca.* 60 s). Data were plotted using relative reflectivity R_E/R_{ref} where R_E is the reflectivity measured at the desired potential and R_{ref} the reflectivity measured at $U = 0.1$ V *vs.* RHE.

2.5. X-ray photoelectron spectroscopy

XPS patterns were obtained on a XR3E2 spectrometer (Vacuum Generator) equipped a Mg K_α (1253.6 eV) X-ray source powered at 300 W (15 kV–20 mA). The kinetic energies of the photoelectrons were measured using a hemispherical electron analyser working in the constant pass energy mode (30.0 eV). The background pressure in the analysis chamber was kept below 10^{-9}–10^{-10} mbar during data acquisition. The XPS data signals were taken in increments of 0.1 eV with dwelling times of 50 ms. Analyses were carried out at an angle of 90° between the sample surface and the analyser. High-resolution spectra envelopes were obtained by curve fitting of synthetic peak components using the software "Avantage" from ThermoSCientific. The raw data was used with no preliminary smoothing. Symmetric Gaussian–Lorentzian (90:10) product functions were used to approximate the line shapes of the fitting components with Shirley background corrections. The full width at half maximum was fixed at 1.7 ± 0.1 eV.

2.6. Raman spectroscopy

Raman spectroscopy was used to probe the extent of graphitization of the fresh/aged carbon supports. The Raman spectra were recorded *ex situ* using a Renishaw RM1000 or a Renishaw In-Via spectrometer. The Raman spectra were obtained by excitation with the radiation from a argon laser (514 nm) operated at approximately 5 mW. The detector was a Peltier-cooled charge coupled device camera (CCD) and the spectral resolution was about 1 cm^{-1}. The measurements were performed with an X50 ULWD objective, and a 100 μm confocal aperture for the sample illumination and collection of the scattered photons.

3. Results and discussion

3.1. Electrochemical characterization

Fig. 1 shows cyclic voltammograms measured on the Pt/C 40 wt. % electrocatalyst before and after aging for 1.5, 2.5 and 3.5 years under open circuit conditions in air atmosphere (see experimental).

In the potential region $0.05 < U < 0.4$ V *vs.* RHE, the features associated with the under-potential deposition/desorption of protons onto/from Pt nanoparticles remain nearly identical, which suggests that the mean Pt crystallite size does not change during the aging test [22]. This result agrees with the minor changes of the surface averaged mean particle size determined by TEM (Table 1). In the potential interval $0.5 < U < 0.8$ V vs. RHE, a broad oxidation peak ($I > 0$) can be distinguished, which we ascribe to electron transfer on quinone/hydroquinone groups [23]:

$$C = O_{(s)} + H^+ + e^- \rightleftarrows C - OH_{(s)}$$

The electrical charge under this peak is increasing on the aged Pt/C electrocatalysts (positive-going potential sweep), pointing towards higher surface coverage with hydroquinone groups. Interestingly, the oxidation peak also shifts towards more positive potential (*ca.* 30 mV), and the reduction peak of quinone-type groups ($U = 0.60$ V vs. RHE) progressively disappears on the aged Pt/C samples. Assuming no pH variation, the positive shift of the oxidation peak may be rationalized by considering that hydroquinone groups experience different chemical environment on the fresh/aged Pt/C electrocatalysts. Indeed, previous studies have shown that a decrease in the number of aromatic rings causes an increase of the quinone/hydroquinone standard potential [23]. In this frame, the observed positive shift might sign the decrease in the number of aromatic rings resulting from the corrosion of the graphite-like crystallites. Another possibility is that the proportion of electron-withdrawing groups, such as carboxyl and anhydride, increases during the corrosion of the HSAC support. However, both scenarios cannot explain the decreased electrical charge under the

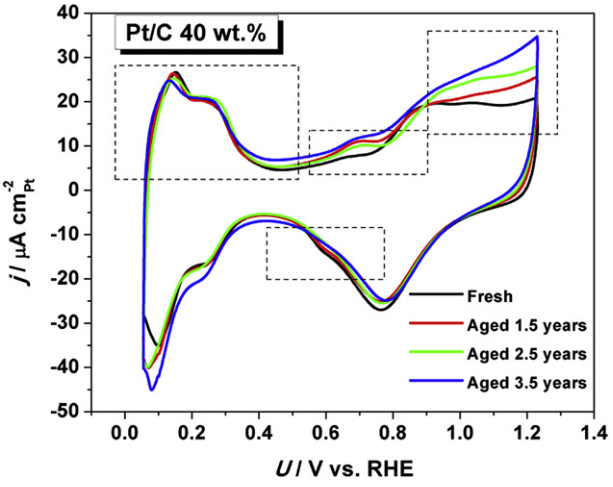

Fig. 1. Cyclic voltammograms measured on Pt/C 40 wt. % after 0, 1.5, 2.5 and 3.5 years under OCP conditions. The current are normalized to the real surface area estimated by CO_{ad} stripping coulometry. Each voltammogram is the average of three measurements. Electrolyte: 0.1 M $HClO_4$; $v = 0.020$ V s^{-1}; $T = 20$ °C.

reduction peak: the latter suggests that hydroquinone groups present on the surface of the aged Pt/C samples are irreversibly oxidized during the potential sweep.

3.2. XPS measurements

The chemical nature of the surface oxygen-containing groups was investigated by XPS. Fig. 2 shows the C1s XPS spectra measured on the fresh/aged Pt/C electrocatalysts. The C1s spectra comprises different peaks at 284.5, 285.6, 287.3 and 289.4 eV associated with C–C (sp^2 and sp^3-hybridized carbon atoms), C–O (hydroxyl, epoxy, phenol and ether), C=O (carbonyl and/or quinone-like), and O–C=O (carboxylic acid, lactone, anhydride) bonds, respectively. Additional peaks at 291.4 and 292.9 eV are ascribed to C–F bonds in the Nafion® ionomer used as binder [11]. The lower binding energy component is assigned to $C–F_2$ groups while the higher binding energy component is ascribed to $C–OF_2$ and/or $C–F_3$ groups [24].

Fig. 2 illustrates that the most pronounced changes are observed in the carbon–carbon and carbon–oxygen related peaks. Assuming slight or no degradation of the perfluorinated ionomer in our experimental conditions [11], the ratio of the $(C–C)/(C–F_2 + C–F_3)$ XPS areas (hereafter referred as the C/F ratio) allows a fast and semi-quantitative monitoring of the carbon content in each sample. Similarly, the O/F ratio allows fast comparison of the total oxygen content. The C/F ratio is continuously decreasing, most severely during the first 1.5 years, indicating fast corrosion of the Vulcan XC72 support. The O/F ratio is also decreasing between 0 and 1.5 years, most severely for C–O-containing functional groups. These results suggest that the oxygen-containing surface groups present on the fresh Vulcan XC 72 are oxidized during the first 1.5 years of aging at OCP. Recent results show that the kinetics of this process are in fact much faster since most of oxygenated groups present on the fresh Vulcan XC72 disappear after *ca.* 2 weeks at OCP (see the C1s XPS spectra in Supplementary Material – Fig. S1). Finally, the slight increase of the O/F ratio observed during the following 2 years is believed to sign slow corrosion of the C–C bonds present in graphite crystallites, and will be confirmed by FTIR and Raman spectroscopy measurements.

3.3. EC-FTIR measurements

The oxygen-containing functional groups present on the surface of the fresh/aged carbon supports were also identified by *in situ* Fourier-transformed infrared spectroscopy measurements. Fig. 3 shows single-beam spectra measured at $U = 0.80$ V *vs.* RHE on the fresh/aged Pt/C electrocatalysts. The FTIR spectra are normalized to a reference spectrum acquired at $U = 0.10$ V *vs.* RHE, a procedure that allows (i) minoring the deformation induced by the O–H vibrational modes of water molecules and (ii) probing the vibrational modes of functional groups formed between $0.1 < U < 0.80$ V *vs.* RHE on the HSAC surface.

Different bands are present in Fig. 3, and their assignment is summarized in Table 2. The weak absorbance bands between 1000 and 1300 cm^{-1} are assigned to the C–O stretching (ν(C–O)) in carboxylic, ether-like, alcoholic and/or phenolic groups [9,25,26]. Those bands are very large confirming the complexity of the chemical environment (presence of aromatic rings and of various oxygen-containing functional groups). The band monitored at $\bar{\nu} = 1385–1390$ cm^{-1} on the fresh Pt/C sample is assigned to the C–O–H bending in carboxyl groups [9]. In the C=O stretching region (ν(C=O)), between 1600 and 1850 cm^{-1}, the band at 1705–1730 cm^{-1} indicates the presence of carbonyl groups of carboxylic acids, or lactone groups [25]. This band is very large and overlaps with the stretching of quinone groups at 1650 and 1670 cm^{-1} [25] and the in-plane bending region of water molecules (δ(O–H)) at $\bar{\nu} \approx 1620–1640$ cm^{-1}. The stretching of CO molecules adsorbed on the Pt surface (ν(C=O)/Pt) is observed at $\bar{\nu} \approx 2000$ cm^{-1}, in agreement with our previous study [9]. Two bands of weak intensity at $\bar{\nu} = 2120$ and 2150 cm^{-1} reveal the presence of ketenes (C=C=O) on the 3.5 years aged Pt/C electrocatalyst [25]. Finally, the asymmetric O=C=O stretching vibration of CO_2 is observed at $\bar{\nu} = 2345$ cm^{-1}.

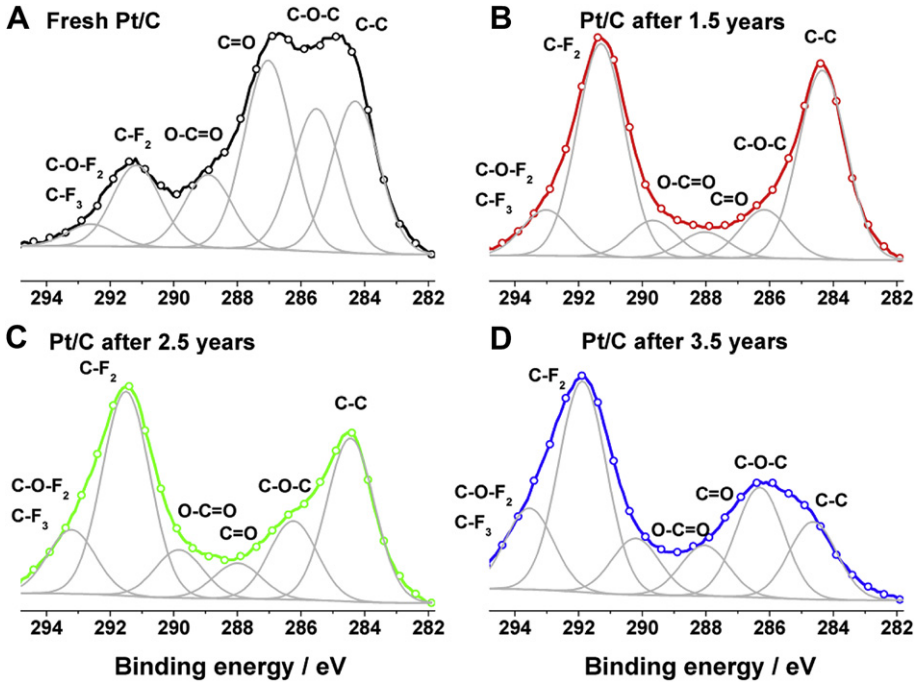

Fig. 2. XPS C1s spectra measured on catalytic layers made of fresh/aged Pt/C powders.

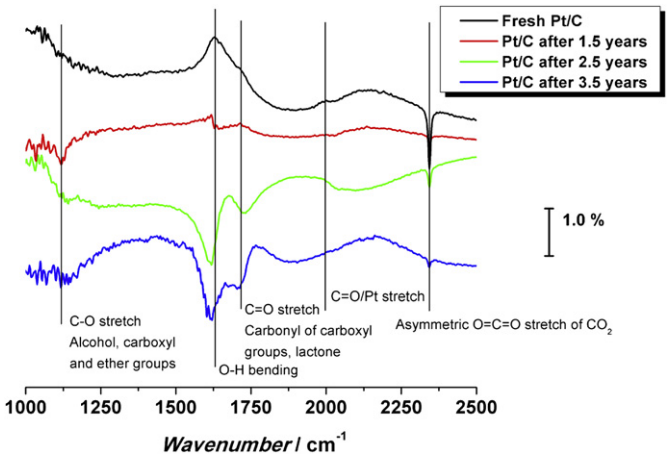

Fig. 3. FTIR spectra acquired *in situ* on catalytic layers made of fresh/aged Pt/C 40 wt. % powders. The reference spectrum was taken at $U = 0.10$ V *vs.* RHE.

Two interesting features emerge from the comparison of the FTIR spectra on the fresh/aged electrocatalysts. Firstly, the chemical nature of the functional groups present on the fresh/aged Pt/C samples is identical (carboxylic, carbonylic, ether, and alcoholic groups). Secondly, the quantity of gaseous CO_2 produced at $U = 0.8$ V *vs.* RHE is maximal on the fresh Pt/C and decreases with an increase in the aging time. Since all measurements were performed under identical experimental conditions (Pt/C loading on the Au electrode, electrolyte, temperature, duration of the potential steps), this suggests that the fresh carbon support is more prone to be oxidized into CO_2 than the aged carbon support. In agreement with this hypothesis, we observed a decreased CO/Pt band intensity at $U = 0.80$ V *vs.* RHE on the aged Pt/C samples. Finally, we noticed that potential stepping from 0.1 to 0.8 V *vs.* RHE induces hydrophobicity/hydrophilicity of the fresh/aged carbon surface, respectively. Indeed, the O–H bending vibrations of water ($\bar{\nu} = 1645$ cm^{-1}) point positively on the fresh Pt/C sample, indicating that water molecules exit the "thin layer" formed between the electrode and the CaF_2 prism when stepping from low to high electrode potential. Conversely, water molecules enter the thin layer during this sequence on the aged Pt/C samples. In other words, the aged carbon surface is more hydrophilic at $U = 0.8$ V *vs.* RHE than at the reference $U = 0.1$ V *vs.* RHE potential. It is also interesting to note that the O–H bending vibration of water molecules redshifts by *ca.* 15 cm^{-1} on the aged Pt/C samples, which indicates that the structure of the water molecules present in the "thin layer" changes from "organized water" (H-bonded) on the fresh Pt/C sample to "free water" on the aged Pt/C samples. Such result is believed to be related to variations in the wettability properties of the carbon support over time, induced by different oxygen content (see Section 2.2) and by different fractions of sp^2 and sp^3 carbon atoms (see Section 2.4) in the fresh/aged Pt/C samples.

Table 2
Proposed functional groups observed on Vulcan XC 72, and their corresponding infrared assignment.

Wavenumber/cm^{-1}	Bond	Mode	Functional group
1115–1120	C–O	Stretching	Carboxylic, ether-like, alcoholic and phenolic
1385–1390	C–O–H	Bending	Carboxylic
1620–1640	O–H	In-plane Bending	Water molecules
1650 and 1670	C=O	Stretching	Quinone
1705–1730	C=O	Stretching	Carbonyl of carboxylic acids, lactone
2000–2030	C=O/Pt	Stretching	Carbon monoxide adsorbed on Pt
2120 and 2150	C=C=O	Stretching	Ketenes
2345	O=C=O	Stretching	Carbon dioxide

3.4. Raman spectroscopy measurements

Raman spectroscopy allows probing the degree of graphitization of the fresh/aged Vulcan XC72 carbon particles [6,27,28]. The vibrational band present at *ca.* 1355 cm^{-1} in Fig. 4, namely the D1 band, is attributed to the amorphous or disordered structure of carbon (sp^3-hybridized carbon atoms), and the G band at *ca.* 1595 cm^{-1} is ascribed to the ordered graphitic domains of the HSAC support (sp^2-hybridized carbon atoms) [29–32]. The slight shoulder at *ca.* 1615 cm^{-1} is ascribed to the D2 band, and corresponds to a defect structure of graphite [28]. On the fresh Pt/C, both the high intensity of the D bands and the broadness of the G band indicate that the carbon support possess a highly disorganized structure that is consistent with the turbostratic structure of Vulcan XC72 [23]. After 1.5 years of aging at OCP, the decreased intensity of the D bands suggests preferential oxidation of the defects of the Vulcan XC72 support (disordered graphitic lattice, graphene layer edges, surface graphene layers). This agrees with the general statement that defect sites are preferentially attacked during the carbon oxidation reaction [33]. After 2.5 years and 3.5 years of aging at OCP, both the D1 band and the G band broaden, indicating that the carbon black support is continuously oxidized during the aging test. The persistence of the D1 band suggests that corrosion also proceeds on the graphite crystallites, in agreement with the XPS measurements that evidenced slight increase of the O/F ratio during this period. These results indicate that the carbon oxidation reaction proceeds fast during the first 1.5 years, most likely on the disordered domains of the Vulcan XC 72 material, and then slows down because the remaining carbon particles possess a more ordered graphitic structure, which is more difficult to oxidize.

3.5. Evolution of the Pt/C structure by electrochemical and electron-based techniques

Finally, we discuss the structural consequences of the carbon corrosion for the supported Pt nanoparticles. Electron microscopy images were used to determine (i) the number and the surface averaged mean Pt particle size, (ii) the density of isolated/aggregated Pt nanoparticles, (iii) the total Pt particle density defined as

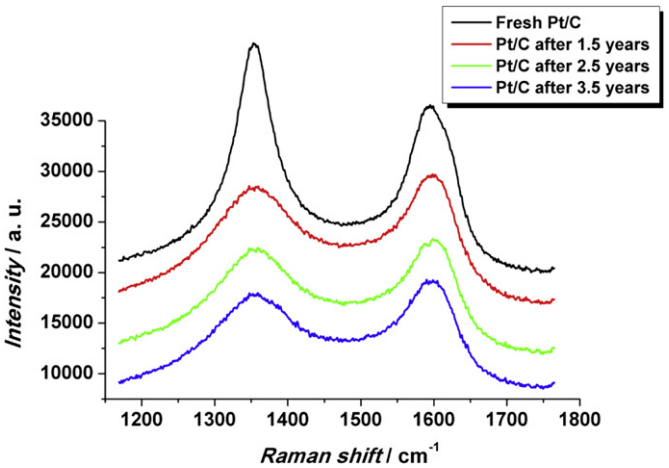

Fig. 4. Selected Raman spectra of the fresh Pt/C electrocatalyst and after 1.5 years, 2.5 years and 3.5 years of aging under OCP conditions.

the sum of isolated and aggregated nanoparticles per μm^2 of the carbon support, (iv) the fraction of aggregated Pt particles and (v) the percentage of isolated Pt particles lost during the durability test. In electrochemistry, we made use of the structure sensitivity of the CO_{ad} electrooxidation reaction to detect *in situ* the aggregation of the carbon-supported Pt particles. Indeed, aggregated Pt particles feature a CO_{ad} electrooxidation pre-peak, which is shifted *ca.* 50 mV negative versus the main CO_{ad} electrooxidation peak (on isolated Pt/C particles) [34–40]. Additionally, the position of the main CO_{ad} stripping peak shifts towards positive potential when decreasing the Pt particle size [34–37].

Fig. 5 shows the background subtracted CO_{ad} stripping voltammograms measured after different life stages: fresh, after 1.5 years, 2.5 years and 3.5 years. Two CO_{ad} electrooxidation peaks can be distinguished on the fresh sample: a broad peak initiating at *ca.* 0.65 V *vs.* RHE, which is composed of different contributions (at $U = 0.69$, 0.72 and 0.75 V *vs.* RHE), and a main peak at *ca.* 0.84–0.85 V *vs.* RHE with some tail on the right-hand side of the peak. Upon aging, the charge under the CO_{ad} electrooxidation pre-peak increases at the expense of the main peak. Concomitantly, the position of the main CO_{ad} electrooxidation peak remains nearly unchanged (slight negative shift of the CO_{ad} electrooxidation from 0.85 to 0.84 V *vs.* RHE). These results indicate an increased fraction of aggregated Pt nanoparticles in the aged Pt/C sample and minor changes of the mean crystallite size, in agreement with the particle size distributions established from TEM images (Fig. 5, right-hand side). They are in agreement with the considerable loss of isolated Pt particles presented in Table 1 (formation of Pt aggregates from "isolated" Pt particles that moved and aggregated upon corrosion of the carbon support). The density of isolated Pt particles decreases by a factor of 4 during the aging sequence, while the fraction of aggregated Pt particles remains nearly identical.

Interestingly, this trend is valid whatever the Pt weight fraction (Fig. 6). CO_{ad} stripping experiments performed on Pt/C 20 wt%, 30 wt. % or 40 wt. % reveal that the charge under the CO_{ad} electrooxidation pre-peak increases at the expense of the main peak. Concomitantly, the position of the main peak remains nearly identical.

The morphological changes of the Pt nanoparticles were quantified by a proper analysis of representative TEM images (Fig. 7). The fraction of isolated Pt particles decreases very fast, this trend being maximal for the catalyst with the highest Pt weight fraction (40 wt. %). Since this catalyst possess the lowest inter-particle distance and the highest Pt/C coverage (calculated as the ratio between the surface area of Pt particles and the surface area of carbon support), the facile aggregation of Pt nanoparticles is not surprising. The density of aggregated Pt particles remains nearly constant over time (within the incertitude of this method) indicating that both isolated and aggregated Pt nanoparticles are detached from the carbon support or that the size of the Pt aggregates increases over time.

3.6. Insights into the carbon corrosion mechanism

The results obtained in this study bridged structural and chemical changes observed during the corrosion of an HSAC support. The decreased C/F and O/F ratios in XPS and the large quantity of gaseous CO_2 produced at $U = 0.80$ V *vs.* RHE on the fresh Pt/C sample in EC-FTIR measurements indicate that the

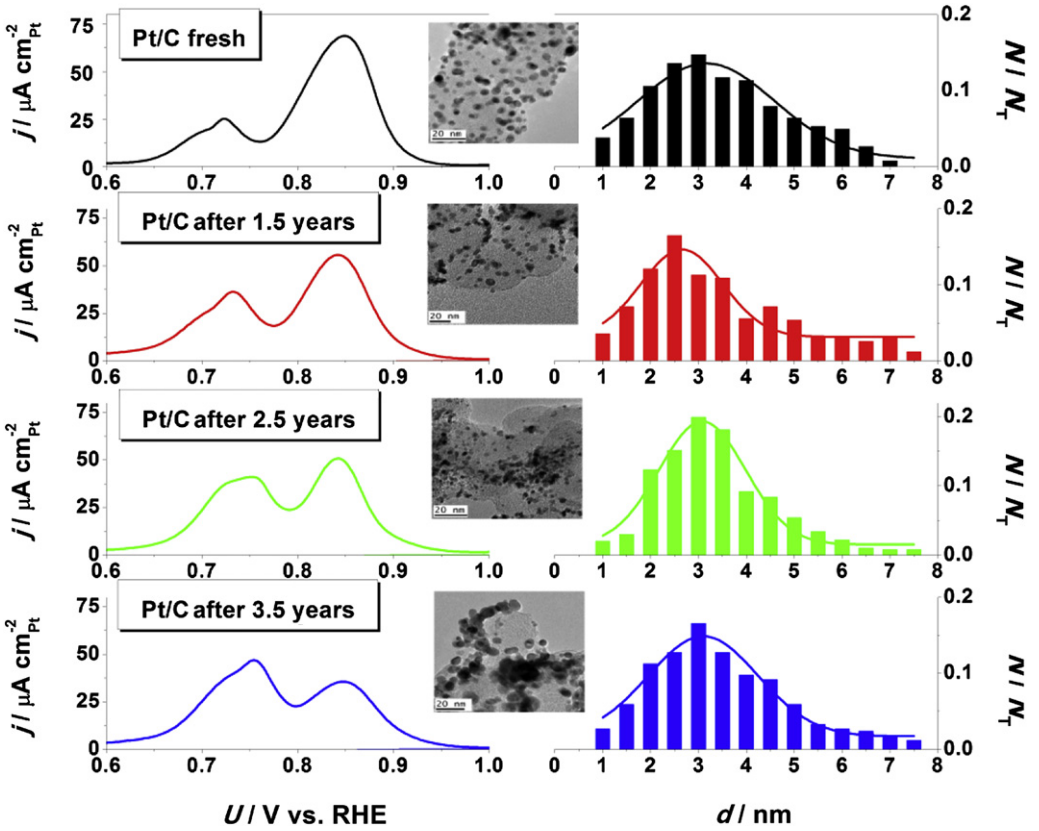

Fig. 5. Averaged background subtracted CO stripping voltammograms (left) and particle size distributions (right) of fresh and aged Pt/C 40 wt. %. Only "isolated" particles (that is non-aggregated, single grain spherical particles) were counted to build the particle size distributions. Representative TEM images of the aged Pt/C catalysts are shown in the insets. The current are normalized to the real surface area estimated by CO_{ad} stripping coulometry. Each voltammogram is the average of three measurements. Electrolyte: 0.1 M $HClO_4$; $v = 0.020$ V s^{-1}; $T = 20$ °C.

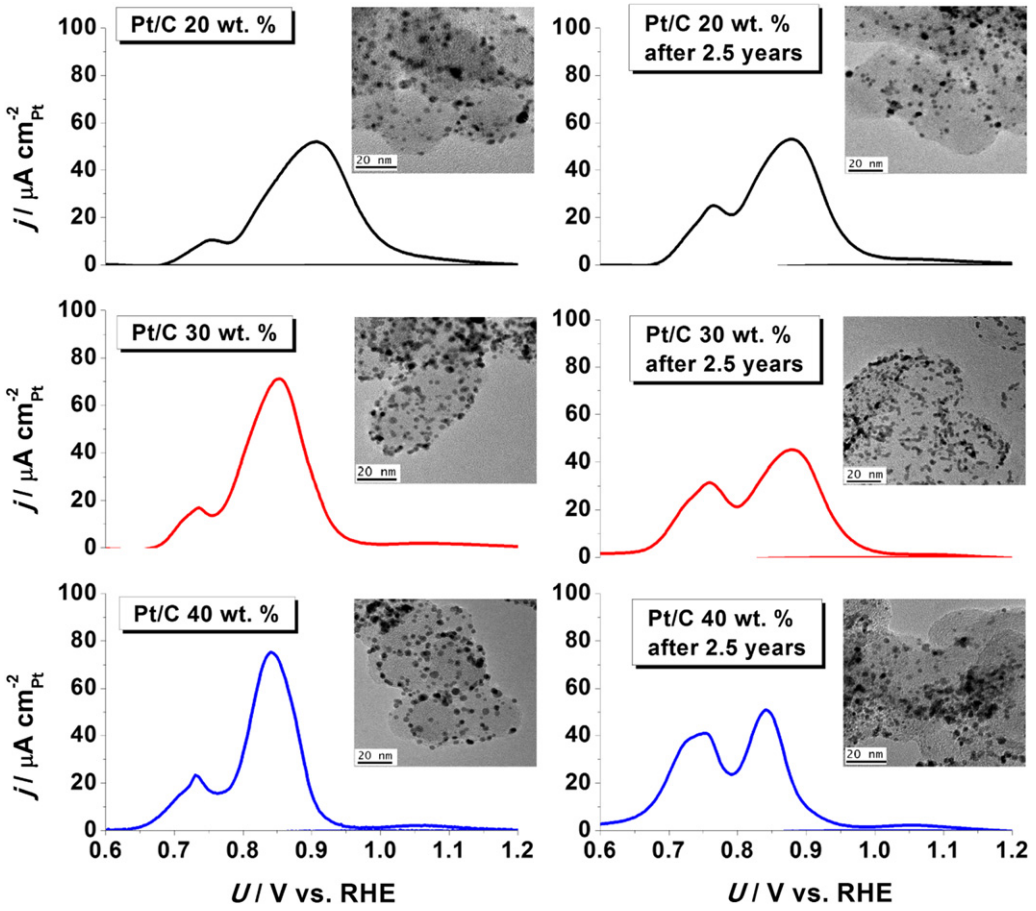

Fig. 6. Averaged background subtracted CO stripping voltammograms and representative TEM pictures of fresh and aged Pt/C catalysts used in study. The current are normalized to the real surface area estimated by CO stripping coulometry. Each voltammogram is the average of three measurements. Electrolyte: 0.1 M $HClO_4$; $v = 0.020$ V s^{-1}; $T = 20$ °C.

oxygen-containing functional groups present on the fresh Vulcan XC72 particles are easily oxidized over the first 1.5 years under OCP conditions in air atmosphere. This nicely agrees with the fast corrosion rates observed on pre-oxidized carbon black materials or carbon nanofibres in the literature [41–43]. Raman measurements (decreased D bands intensity over the first 1.5 years) provide evidences that these oxidized domains are associated with disordered domains of the carbon support and defects sites of the graphitic lattice. In the second stage of the COR, the organized domains of the HSAC support (graphitic carbon, sp^2-hybridized) are also oxidized, the rate of this process being much smaller than that observed on the non-graphitic regions of the HSAC support. The corrosion of the organized domains of the carbon support produces mostly CO_{surf} groups as indicated by XPS and EC-FTIR measurements, and to a minor extent, CO_2 molecules at $U = 0.80$ V *vs.* RHE. This translates by the persistence of the D1 band in Raman measurements. As a consequence of the COR catalysis by Pt, the nanometre-sized Pt particles move and detach from the HSAC support, as evidenced by combined electron microscopy and electrochemical techniques.

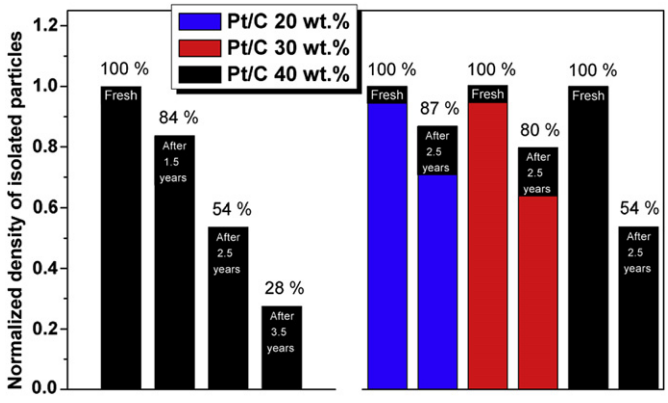

Fig. 7. Normalized density of isolated particles for fresh and aged Pt/C catalysts having different Pt weight fractions.

4. Conclusions

The high surface area carbon supports used in proton-exchange membrane fuel cells are not inert materials. Due to their turbostratic structure, they possess a large variety of oxygen-bearing carbon surface groups identified as hydroxyl, phenol, ether, carbonyl, and carboxyl by deconvolution of the X-ray photoelectron peaks and Fourier-Transformed infrared spectroscopy bands. Upon aging under OCP conditions, the disordered domains of the HSAC support (non-graphitic, sp^3-hybridized) are first oxidized. This translates by large production of gaseous CO_2 at PEMFC relevant cell voltage in FTIR measurements ($U = 0.80$ V *vs.* RHE). In the second stage of the Vulcan XC72 corrosion reaction, Raman spectroscopy measurements indicate that the ordered domains (graphitic carbon, sp^2-hybridized) are also oxidized, the rate of this process being much smaller than that of the non-graphitic regions. The corrosion of the organized domains produces mostly CO_{surf} groups, and to a minor extent, CO_2 molecules at $U = 0.80$ V *vs.* RHE. Electron microscopy and electrochemical techniques reveal a continuous loss of nm-sized Pt particles over

time, which is rationalized on the basis of the Pt-catalysed carbon corrosion.

Appendix A. Supplementary material

Supplementary material related to this article can be found at http://dx.doi.org/10.1016/j.jpowsour.2012.12.053.

References

[1] W. Vielstich, A. Lamm, H.A. Gasteiger, in: John Wiley & Sons, Chichester, 2003.
[2] E. Guilminot, A. Corcella, F. Charlot, F. Maillard, M. Chatenet, J. Electrochem. Soc. 154 (2007) B96–B105.
[3] Z. Zhao, L. Dubau, F. Maillard, J. Power Sources 217 (2012) 449–458.
[4] K.J.J. Mayrhofer, J.C. Meier, S.J. Ashton, G.K.H. Wiberg, F. Kraus, M. Hanzlik, M. Arenz, Electrochem. Com. 10 (2008) 1144–1147.
[5] J.C. Meier, C. Galeano, I. Katsounaros, A.A. Topalov, A. Kostka, F. Schüth, K.J.J. Mayrhofer, ACS Catal. 2 (2012) 832–843.
[6] T. Yoda, H. Uchida, M. Watanabe, Electrochim. Acta 52 (2007) 5997–6005.
[7] S. Maass, F. Finsterwalder, G. Frank, R. Hartmann, C. Merten, J. Power Sources 176 (2008) 444–451.
[8] Z.Y. Liu, J.L. Zhang, P.T. Yu, J.X. Zhang, R. Makharia, K.L. More, E.A. Stach, J. Electrochem. Soc. 157 (2010) B906–B913.
[9] F. Maillard, A. Bonnefont, F. Micoud, Electrochem. Commun. 13 (2011) 1109–1111.
[10] N. Linse, L. Gubler, G.G. Scherer, A. Wokaun, Electrochim. Acta 56 (2011) 7541–7549.
[11] E. Guilminot, A. Corcella, C. Iojoiu, G. Berthomé, F. Maillard, M. Chatenet, J.-Y. Sanchez, J. Electrochem. Soc. 154 (2007) B1106–B1114.
[12] R. Borup, J. Meyers, B. Pivovar, Y.S. Kim, R. Mukundan, N. Garland, D. Myers, M. Wilson, F. Garzon, D. Wood, P. Zelenay, K. More, K. Stroh, T. Zawodzinski, J. Boncella, J.E. McGrath, M. Inaba, K. Miyatake, M. Hori, K. Ota, Z. Ogumi, S. Miyata, A. Nishikata, Z. Siroma, Y. Uchimoto, K. Yasuda, K.I. Kimijima, N. Iwashita, Chem. Rev. 107 (2007) 3904–3951.
[13] Y. Shao-Horn, W. Sheng, S. Chen, P. Ferreira, E. Holby, D. Morgan, Top. Catal. 46 (2007) 285–305.
[14] L. Dubau, L. Castanheira, G. Berthomé, F. Maillard, Electrochim. Acta (2013). submitted to the special Issue of Electrochimica Acta dedicated to the 63rd meeting of the ISE.
[15] L.M. Roen, C.H. Paik, T.D. Jarvi, Electrochem. Solid-State Lett. 7 (2004) A19–A22.
[16] K.H. Kangasniemi, D.A. Condit, T.D. Jarvi, J. Electrochem. Soc. 151 (2004) E125–E132.
[17] S. Zhang, X.-Z. Yuan, R. Hiesgen, K.A. Friedrich, H. Wang, M. Schulze, A. Haug, H. Li, J. Power Sources 205 (2012) 290–300.
[18] C.A. Reiser, L. Bregoli, T.W. Patterson, J.S. Yi, J.D.L. Yang, M.L. Perry, T.D. Jarvi, Electrochem. Solid-State Lett. 8 (2005) A273–A276.
[19] J. Willsau, J. Heitbaum, J. Electroanal. Chem. 161 (1984) 93–101.
[20] M.F. Mathias, R. Makharia, H. Gasteiger, J.J. Conley, T.J. Fuller, G.J. Gittleman, S.S. Kocha, D.P. Miller, C.K. Mittelsteadt, T. Xie, S.G. Yan, P.T. Yu, Interface 14 (2005) 24–35.
[21] F. Micoud, F. Maillard, A. Bonnefont, N. Job, M. Chatenet, Phys. Chem. Chem. Phys. 12 (2010) 1182–1193.
[22] F. Maillard, S. Pronkin, E.R. Savinova, Influence of size on the electrocatalytic activities of supported metal nanoparticles in fuel cells related reactions, in: W. Vielstich, H.A. Gasteiger, H. Yokokawa (Eds.), Handbook of Fuel Cells – Fundamentals, Technology and Applications, John Wiley & Sons, Inc., New York, 2009, pp. 91–111.
[23] K. Kinoshita, Carbon, Electrochemical and Physicochemical Properties, John Wiley & Sons, New York, 1988.
[24] V. Parry, G. Berthomé, J.C. Joud, O. Lemaire, A.A. Franco, J. Power Sources 196 (2011) 2530–2538.
[25] P.E. Fanning, M.A. Vannice, Carbon 31 (1993) 721–730.
[26] R.M. Silverstein, F.X. Webster, D.J. Kiemle, Spectrometric Identification of Organic Compounds, seventh ed., John Wiley & Sons, Chichester, 2005.
[27] Y. Hiramitsu, H. Sato, H. Hosomi, Y. Aoki, T. Harada, Y. Sakiyama, Y. Nakagawa, K. Kobayashi, M. Hori, J. Power Sources 195 (2010) 435–444.
[28] M. Hara, M. Lee, C.-H. Liu, B.-H. Chen, Y. Yamashita, M. Uchida, H. Uchida, M. Watanabe, Electrochim. Acta 70 (2012) 171–181.
[29] F. Tuinstra, J.L. Koenig, J. Chem. Phys. 53 (1970) 1126–1130.
[30] Y. Wang, D.C. Alsmeyer, R.L. McCreery, Chem. Mater. 2 (1990) 557–563.
[31] A. Sadezky, H. Muckenhuber, H. Grothe, R. Niessner, U. Pöschl, Carbon 43 (2005) 1731–1742.
[32] M. Marcinek, L.J. Hardwick, G.Z. Żukowska, R. Kostecki, Carbon 48 (2010) 1552–1557.
[33] O.V. Cherstiouk, A.N. Simonov, N.S. Moseva, S.V. Cherepanova, P.A. Simonov, V.I. Zaikovskii, E.R. Savinova, Electrochim. Acta 55 (2010) 8453–8460.
[34] F. Maillard, M. Eikerling, O.V. Cherstiouk, S. Schreier, E. Savinova, U. Stimming, Faraday Discuss. 125 (2004) 357–377.
[35] F. Maillard, E. Savinova, P.A. Simonov, V.I. Zaikovskii, U. Stimming, J. Phys. Chem. B 108 (2004) 17893–17904.
[36] F. Maillard, S. Schreier, M. Hanzlik, E.R. Savinova, S. Weinkauf, U. Stimming, Phys. Chem. Chem. Phys. 7 (2005) 385–393.
[37] F. Maillard, E.R. Savinova, U. Stimming, J. Electroanal. Chem. 599 (2007) 221–232.
[38] O.V. Cherstiouk, A.N. Gavrilov, L.M. Plyasova, I.Y. Molina, G.A. Tsirlina, E.R. Savinova, J. Solid State Electrochem. 12 (2008) 497–509.
[39] E.G. Ciapina, S.F. Santos, E.R. Gonzalez, J. Electroanal. Chem. 644 (2010) 132–143.
[40] A. Lopez-Cudero, J. Solla-Gullon, E. Herrero, A. Aldaz, J.M. Feliu, J. Electroanal. Chem. 644 (2010) 117–126.
[41] P.L. Antonucci, L. Pino, N. Giordano, L. Pinna, Mater. Chem. Phys. 21 (1989) 495–506.
[42] N. Giordano, P.L. Antonucci, E. Passalacqua, L. Pino, A.S. Arico, K. Kinoshita, Electrochim. Acta 36 (1991) 1931–1935.
[43] H.S. Oh, K. Kim, Y.J. Ko, H. Kim, Int. J. Hydrogen Energy 35 (2010) 701–708.